

Multi-soliton interactions underlying the dynamics of breather rogue waves

D. S. Agafontsev,^{1,2} A. A. Gelash,³ S. Randoux,⁴ and P. Suret⁴

¹*Shirshov Institute of Oceanology of RAS, 117997, Moscow, Russia*

²*Department of Mathematics, Physics and Electrical Engineering,
Northumbria University, Newcastle upon Tyne, NE1 8ST, United Kingdom*

³*Laboratoire Interdisciplinaire Carnot de Bourgogne (ICB),*

UMR 6303 CNRS – Université Bourgogne Franche-Comté, 21078 Dijon, France

⁴*Univ. Lille, CNRS, UMR 8523 - PhLAM - Physique des Lasers Atomes et Molécules, F-59000 Lille, France*

We consider the most famous one-breather solutions of the focusing one-dimensional nonlinear Schrödinger equation which are used in the theory of rogue waves – the Peregrine, Akhmediev and Kuznetsov-Ma breathers, as well as the general case of drifting Tajiri-Watanabe breather. In terms of the inverse scattering transform (IST) theory, it is known that these breathers are constructed by “dressing” a plane wave solution with a single soliton. In this construction, we replace the plane wave with an exact N -soliton solution which converges asymptotically to the plane wave at large number of solitons N . As a result, we obtain exact $(N + 1)$ -soliton solutions practically indistinguishable from the Peregrine, Akhmediev, Kuznetsov-Ma and Tajiri-Watanabe breathers in a relatively wide region of space and time. The constructed solutions are localized in space with characteristic width proportional to N and approximate the breathers with accuracy improving as N grows. Our method makes it possible to build solitonic models with the same dynamical properties for the higher-order rational and super-regular breathers, and can be generalized straightforwardly to multi-breather solutions, breathers on a nontrivial background (e.g., cnoidal waves) and other integrable systems.

I. INTRODUCTION

The phenomenon of rogue waves – unusually large waves that appear suddenly from moderate wave background – has been extensively studied in the recent years. A number of mechanisms have been suggested to explain their emergence, see e.g. reviews [1–4], with one of the most general ideas being that rogue waves could be related to breather-type solutions of the underlying nonlinear evolution equations [5–8]. A particular example of a nonlinear mathematical model suitable for the description of rogue waves is the one-dimensional nonlinear Schrödinger equation (1D-NLSE) of the focusing type,

$$i\psi_t + \frac{1}{2}\psi_{xx} + |\psi|^2\psi = 0, \quad (1)$$

which describes evolution of a narrowband signal in a weakly nonlinear media and is widely applicable in different fields of studies ranging from nonlinear optics to hydrodynamics and Bose-Einstein condensates [9–11]. Several exact solutions of this equation have been suggested as candidates of rogue waves, including the Peregrine [12], Akhmediev [13] and Kuznetsov-Ma [14, 15] breathers, which represent special cases of the Tajiri-Watanabe breather [16]. Taking specific and carefully designed initial conditions, these solutions were reproduced in well-controlled experiments performed in different physical systems [17–23].

Meanwhile, there are certain inconsistencies in describing rogue waves with breathers. First, in many physically relevant situations, the wavefields are localized, as spatial dimensions are typically confined and signal time series have beginning and end. In such systems, breather solutions cannot formally exist, since they have finite-background boundary conditions. This means that the

observed breather-like dynamics, in fact, is achieved by a combination of nonlinear dispersive waves and solitons – the types of nonlinear structures compatible with the vanishing boundary conditions. Secondly, the modeling of rogue waves with breathers typically implies certain scenarios of their emergence, such as in the beginning of nonlinear stage of modulational instability (MI) [8, 13]. However, breather-like rogue waves also appear randomly from time to time long after the MI is fully developed [24], or in the long-time evolution from partially coherent waves [25]. It is unclear how such situations could be potentially modeled with breathers. Finally, the similarity between certain breather profiles and interacting solitons [24, 26, 27] observed in integrable systems, as well as the fission of breather solutions [28, 29] into solitons in nonintegrable systems, also implies a close relationship between breathers and solitons.

In this paper, we aim to address some of these inconsistencies and observations by presenting a universal method for modeling the breather-like dynamics with exact multi-soliton solutions. Our approach is based on the integrability of the 1D-NLSE in terms of the *inverse scattering transform* (IST) theory and on the dressing method also known as the Darboux transformation. Namely, breathers are constructed by “dressing” a plane wave solution $\psi = A e^{i|A|^2 t}$ of Eq. (1) with solitons. In this construction, we replace the plane wave with its solitonic model [30], which represents a specific exact N -soliton solution converging asymptotically to the plane wave at large number of solitons N . As a result, we obtain exact multi-soliton solutions which approximate breathers locally very well even for a rather small number of solitons $N \sim 10$. At large N , the constructed solutions turn out to be practically indistinguishable from the breathers in a wide region of space and time.

From a mathematical point of view, our method assumes the continuity of the dressing procedure, when the same dressing of two similar solutions leads to the similar results. We think that it can be generalized straightforwardly to multi-breather solutions, breathers on a non-trivial background (e.g., cnoidal waves), and other integrable systems including vector breathers [31–36].

The paper is organized as follows. In Section II, we discuss in general the dressing method procedure, the soliton and breather solutions, and the solitonic model of the plane wave [30]. In Section III, we construct solitonic models of the Peregrine, Akhmediev, Kuznetsov-Ma and Tajiri-Watanabe breathers, and numerically verify that they approximate these breathers exceptionally well in a wide region of space and time. The final Section IV contains conclusions and discussion. In the Appendix, we provide a detailed description of the dressing method and build solitonic models for the higher-order rational [37] and super-regular [38–40] breathers.

II. DRESSING METHOD CONSTRUCTION

A. Integrability and the dressing method

The 1D-NLSE belongs to a class of nonlinear partial differential equations (PDEs) integrable by means of the IST method. The latter is based on the representation of a PDE as a compatibility condition of an over-determined auxiliary linear system – the Lax pair [41, 42]. For the case of the 1D-NLSE, the Lax pair is known as the Zakharov-Shabat (ZS) system [43] for a two-component vector wave function $\Phi(x, t, \lambda) = (\phi_1, \phi_2)^T$,

$$\Phi_x = \begin{pmatrix} -i\lambda & \psi \\ -\psi^* & i\lambda \end{pmatrix} \Phi, \quad (2)$$

$$\Phi_t = \begin{pmatrix} -i\lambda^2 + \frac{i}{2}|\psi|^2 & \lambda\psi + \frac{i}{2}\psi_x \\ -\lambda\psi^* + \frac{i}{2}\psi_x^* & i\lambda^2 - \frac{i}{2}|\psi|^2 \end{pmatrix} \Phi, \quad (3)$$

where the star stands for the complex conjugate and Eq. (1) is obtained as a compatibility condition $\Phi_{xt} = \Phi_{tx}$. The first equation of the ZS system can be rewritten as an eigenvalue problem for a complex-valued spectral parameter $\lambda = \xi + i\eta$,

$$\widehat{\mathcal{L}}\Phi = \lambda\Phi, \quad \widehat{\mathcal{L}} = i \begin{pmatrix} 1 & 0 \\ 0 & -1 \end{pmatrix} \frac{\partial}{\partial x} - i \begin{pmatrix} 0 & \psi \\ \psi^* & 0 \end{pmatrix}. \quad (4)$$

Similarly to the Schrödinger operator in quantum mechanics [44], the scattering problem (4) for the ZS operator $\widehat{\mathcal{L}}$ and wave function Φ can be introduced, in which the wavefield ψ of the 1D-NLSE plays the role of a potential. For localized potentials, this problem has bounded solutions for real-valued spectral parameter $\lambda = \xi \in \mathbb{R}$ (continuous spectrum), and also for a finite number of discrete points $\lambda_n = \xi_n + i\eta_n$, $\eta_n > 0$, $n = 1, \dots, N$ (discrete spectrum). Note that, without loss of generality, we consider only the upper half of the λ -plane, $\eta = \text{Im } \lambda \geq 0$.

Most importantly, the potential $\psi(x, t)$ turns out to be in one-to-one correspondence with the so-called *scattering data* – a combination $\{\lambda_n, \rho_n(t), r(\xi, t)\}$ of the discrete spectrum points λ_n , associated with them coefficients $\rho_n(t)$, and reflection coefficient $r(\xi, t)$ representing the continuous spectrum – and this scattering data changes trivially over time. In particular, the 1D-NLSE evolution preserves the discrete spectrum, $\partial_t \lambda_n = 0$, while $\rho_n(t)$ and $r(\xi, t)$ evolve exponentially like the Fourier harmonics in the linear waves theory. These properties make it possible to fundamentally solve the Cauchy initial value problem for the 1D-NLSE by finding the scattering data from the solution of the scattering problem (4), calculating its evolution in time, and recovering the potential ψ with the inverse scattering transform. Note, however, that both the direct and inverse scattering transforms represent highly nontrivial nonlinear problems. In particular, the IST is done by solving the integral Gelfand-Levitan-Marchenko equations [42] and can be calculated analytically only in special cases, asymptotically at large time $t \rightarrow \pm\infty$, or in the semiclassical approximation [45, 46].

Like the Fourier spectrum in the linear waves theory, the scattering data is used to characterize the potential $\psi(x, t)$: the reflection coefficient $r(\xi, t)$, representing the continuous spectrum $\lambda = \xi \in \mathbb{R}$, describes the nonlinear dispersive waves, while the discrete eigenvalues λ_n together with the coefficients $\rho_n(t)$ correspond to solitons. In particular, the eigenvalues $\lambda_n = \xi_n + i\eta_n$ contain information about the (invariant in time) soliton amplitudes $a_n = 2\eta_n$ and velocities $v = -2\xi_n$, while the coefficients $\rho_n(t)$ – about their (evolving) position in space and complex phase. In the present paper, we pay special attention to reflectionless potentials $r(\xi, t) = 0$, i.e., solutions of the 1D-NLSE that contain only solitons.

The dressing method (DM) [42, 47], also known as the Darboux transformation [47, 48], is a simplified version of the conventional IST approach. It represents an algebraic scheme for constructing new exact solutions to integrable PDEs by “dressing” a bare solution, and is often used to find general multi-soliton and multi-breather solutions of the 1D-NLSE, see e.g. [39, 48–50]. Here we discuss the DM optimized for dressing with solitons. Note that for this task the DM requires far fewer arithmetic operations than the standard IST method, that makes it favorable when the number of solitons is large [26, 51, 52].

The DM is performed at a specific moment of time which we fix to zero $t = 0$ for simplicity. It starts from an initial background potential $\psi_0(x, t)$ (bare solution) and the corresponding 2×2 matrix solution $\Phi_0(x, t, \lambda)$ of the ZS system (wave function) constructed from two linearly independent solutions of Eqs. (2)-(3). At the n -th step of the recursive procedure, the potential ψ_n and wave function Φ_n dressed with n solitons $\{\lambda_1, \dots, \lambda_n\}$ are obtained as an algebraic transformation of ψ_{n-1} and Φ_{n-1} dressed with $(n-1)$ solitons $\{\lambda_1, \dots, \lambda_{n-1}\}$, see Appendix A 1 for details. This algebraic transformation depends on the eigenvalue of the n -th soliton λ_n and is

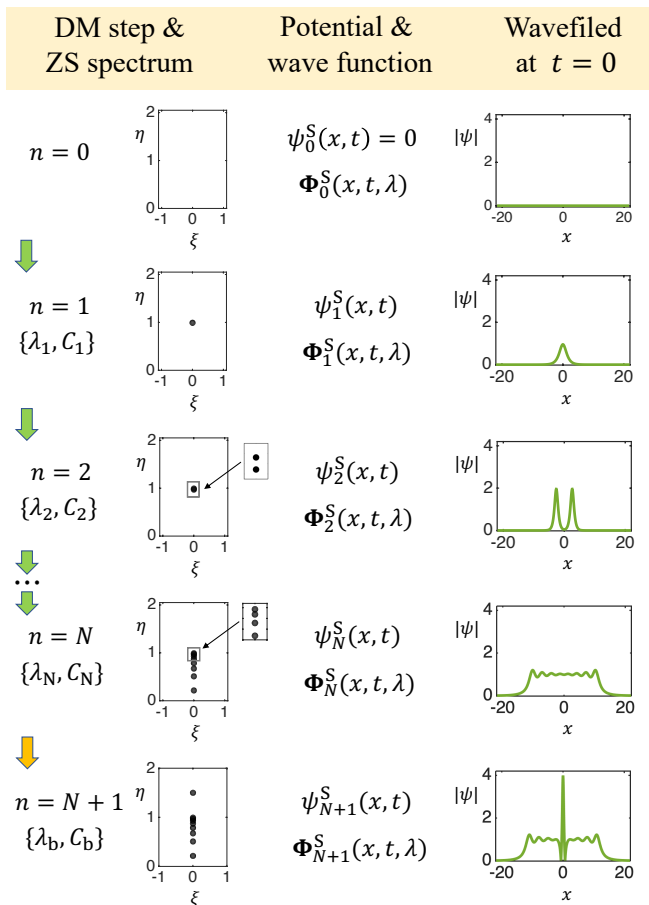


FIG. 1. (Color on-line) Schematic representation of the DM for constructing exact multi-soliton solutions. The left column shows the step number n , the soliton $\{\lambda_n, C_n\}$ used for dressing at this step, and the resulting eigenvalue spectrum of the ZS system (4) in the upper half of the λ -plane. The center column indicates the potential $\psi_n^S(x, t)$ and wave function $\Phi_n^S(x, t, \lambda)$ constructed at this step, while the right column illustrates the absolute value of the potential $|\psi_n^S|$ at $t = 0$. Note that, for solitonic models of breathers, λ_{n-1} and λ_n are very close to each other at small n ; see the zoom of the ZS spectrum shown for the steps $n = 2$ and N . Also note that, at the step $(N + 1)$, the soliton is designated as $\{\lambda_b, C_b\}$ for the subsequent comparison with breather solutions.

defined up to an arbitrary constant $C_n \in \mathbb{C} \setminus \{0\}$, which we will call the norming constant. Note that the dressing procedure is local, i.e., ψ_n and Φ_n depend on ψ_{n-1} and Φ_{n-1} taken at the same point (x, t) .

B. Soliton and breather solutions

An exact N -soliton potential ψ_N^S is constructed from (i) the zero background $\psi_0^S(x, t) = 0$ and (ii) the corresponding wave function $\Phi_0^S(x, t, \lambda)$ which is analytic everywhere in the λ -plane. Each step of the DM leads to the new potential ψ_n^S and new wave function Φ_n^S , and

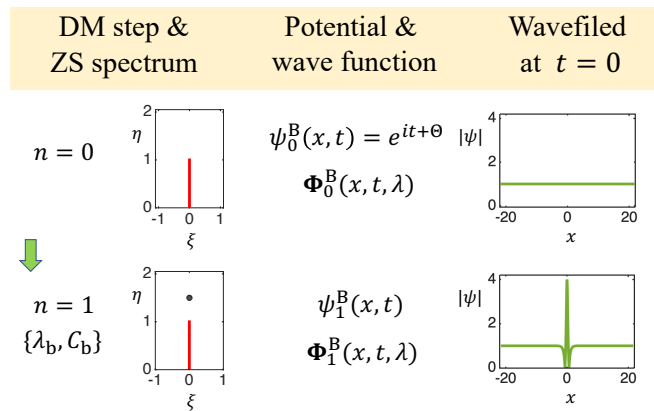


FIG. 2. (Color on-line) Same as in Fig. 1 for the construction of one-breather solutions. The red line in the diagrams of the ZS spectrum shows the cut $[0, i]$, where all wave functions $\Phi_n^B(x, t, \lambda)$ have non-analytic behavior.

consists in adding one soliton λ_n to ψ_{n-1}^S and one pole at $\lambda = \lambda_n$ to Φ_{n-1}^S (we consider only the upper half of the λ -plane). This procedure is schematically illustrated in Fig. 1, where the last soliton is designated as $\{\lambda_b, C_b\}$ for subsequent comparison with breather solutions.

If one parametrizes the norming constants C_n via the soliton position $x_n \in \mathbb{R}$ and phase $\theta_n \in \mathbb{R}$ as

$$C_n = \exp [i\pi + 2i\lambda_n x_n + i\theta_n], \quad (5)$$

then the one-soliton potential takes the following form,

$$\psi_1^S(x, t) = a_1 \frac{\exp [iv_1(x - x_1) + \frac{i(a_1^2 - v_1^2)t}{2} + i\theta_1]}{\cosh a_1(x - v_1 t - x_1)}, \quad (6)$$

where $a_1 = 2\eta_1$ and $v_1 = -2\xi_1$ are the soliton amplitude and velocity. Note that parametrization (5) serves only for a convenient and physically intuitive representation of multi-soliton solutions, and that x_n and θ_n coincide with the observed in the physical space position and phase of a soliton only for one-soliton potential. In presence of other solitons or dispersive waves, the observed position and phase may differ considerably from these parameters.

An exact N -breather potential ψ_N^B is constructed from (i) the plane wave background $\psi_0^B(x, t) = e^{it+i\Theta}$ and (ii) the corresponding wave function $\Phi_0^B(x, t, \lambda)$ which is analytic everywhere in the λ -plane except for the cut $[-i, i]$. Here $\Theta \in \mathbb{R}$ is the initial phase and we consider the plane wave of unit amplitude, since other cases can be obtained with rescaling $t \rightarrow A^2 t$, $x \rightarrow Ax$ and $\psi \rightarrow \psi/A$. As we have noted in Section II A, we consider only the upper half of the λ -plane, so that from now on we will refer to the cut as $[0, i]$. The dressing procedure preserves the non-analytic behavior of the wave function on it, adding at each step one breather to the potential and one pole at $\lambda = \lambda_n$ to the wave function. A schematic representation of the DM for one-breather solutions is shown in Fig. 2. Note that the plane wave and the resulting N -breather potentials are not localized and need to be considered by

the quasi-periodic analogue of the IST called the finite-gap theory [7, 42]. However, the DM is based on a more general Lax pair representation and can still be used for constructing such solutions.

Depending on the choice of the soliton eigenvalue relative to the cut $[0, i]$, a general one-breather potential represents one of the four different cases (i) $\lambda_b = i$, (ii) $\lambda_b = i\eta_b$ with $\eta_b < 1$, (iii) $\lambda_b = i\eta_b$ with $\eta_b > 1$ and (iv) $\text{Re } \lambda_b \neq 0$, corresponding to the Peregrine, Akhmediev, Kuznetsov-Ma and Tajiri-Watanabe breathers respectively. Here we have changed the subscript to reflect that soliton λ_b is used for dressing the plane wave. Below we provide relations for the first three breathers, using the initial phase $\Theta = \pi$ and the norming constant $C_b = 1$ leading to the canonical form of the breathers. The corresponding relations for arbitrary Θ and C_b , together with the relation for the Tajiri-Watanabe breather, are given in Appendixes A 2 and A 3.

The Peregrine breather is obtained by dressing with soliton $\lambda_b = i$,

$$\psi^P(x, t) = e^{it} \left(1 - \frac{4(1 + 2it)}{1 + 4x^2 + 4t^2} \right), \quad (7)$$

and describes a rational perturbation localized both in space and in time, living on the background of the plane wave e^{it} . Note that the additional phase shift $e^{i\pi}$ relative to the bare solution $\psi_0^B = -e^{it}$ appears at every new step of the dressing procedure, see Appendix A 3 for details. The Peregrine breather (7) reaches maximum amplitude $|\psi^P| = 3$ at the point $(0, 0)$.

The Akhmediev breather is constructed by dressing with soliton $\lambda_b = i\eta_b$, $\eta_b < 1$,

$$\psi^A(x, t) = e^{it} \left(1 - \frac{2\kappa^2 \cosh \Omega_A t + i\Omega_A \sinh \Omega_A t}{\cosh \Omega_A t - \eta_b \cos 2\kappa x} \right), \quad (8)$$

where $\kappa = \sqrt{1 - \eta_b^2}$ and $\Omega_A = 2\eta_b \kappa$. It describes a spatially periodic perturbation with period π/κ on the background of the plane wave e^{it} ; this perturbation becomes most pronounced at the time $t = 0$ and vanishes within the characteristic time Ω_A^{-1} as $t \rightarrow \pm\infty$.

The Kuznetsov-Ma breather is obtained by dressing with soliton $\lambda_b = i\eta_b$, $\eta_b > 1$,

$$\psi^{\text{KM}}(x, t) = e^{it} \left(1 - \frac{2\nu^2 \cos \Omega_K t + i\Omega_K \sin \Omega_K t}{\eta_b \cosh 2\nu x - \cos \Omega_K t} \right), \quad (9)$$

where $\nu = \sqrt{\eta_b^2 - 1}$ and $\Omega_K = 2\eta_b \nu$. It describes a standing localized perturbation of the plane wave e^{it} ; this perturbation has characteristic width $(2\nu)^{-1}$ in space and oscillates with period $2\pi/\Omega_K$ in time.

The Tajiri-Watanabe breather corresponds to a general case when a plane wave is dressed by a moving soliton $\lambda_b = \xi_b + i\eta_b$ with $|\xi_b| \neq 0$ and $\eta_b > 0$. This breather describes a perturbation of a plane wave moving with a constant group velocity in space and oscillating with a specific period in time, see [16, 53] for details. Note

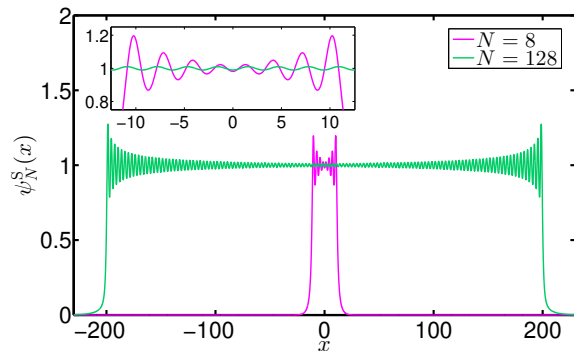


FIG. 3. (Color on-line) Solitonic model (11)-(12) of the plane wave $\psi_0^B = e^{it+i\Theta}$ for $N = 8$ (magenta) and $N = 128$ (green), at the initial time $t = 0$ and for the initial phase $\Theta = 0$.

that this solution has different phases of the plane wave background to the left and to the right of itself,

$$\lim_{x \rightarrow \pm\infty} \frac{\psi^{\text{TW}}(x, t)}{e^{it+i\Theta+i\pi}} = \exp \left(\pm 2i \arg[i(\zeta_b + \lambda_b)] \right), \quad (10)$$

where $\zeta_b = \sqrt{\lambda_b^2 + 1}$. This means that, on the background of the plane wave, this breather describes a perturbation that is formally not localized.

C. Solitonic model of the plane wave solution

In [30], we have developed a solitonic model of the plane wave $\psi_0^B = e^{it+i\Theta}$, which represents an exact N -soliton solution (N -SS) converging asymptotically to ψ_0^B at large number of solitons N . This N -SS contains standing solitons with eigenvalues $\lambda_n \in (0, i)$, see also [54–57],

$$\left\{ \{ \lambda_n \} = \{ i\eta_n \} \mid \tan(L\sqrt{1 - \eta_n^2}) = -\frac{\sqrt{1 - \eta_n^2}}{\eta_n}, \right. \\ \left. 0 < \eta_n < 1, \quad n = 1, \dots, N \right\}, \quad (11)$$

where $L = \pi(N - 1/4)$ is the characteristic width of this solution in the physical space. For eigenvalues sorted in *descending* order, $\eta_m < \eta_l$ for $m > l$, the norming constants take the following simple form,

$$C_n = e^{i\pi n + i\Theta}, \quad (12)$$

and correspond to solitons sitting at the coordinate origin $x_n = 0$ with phases $\theta_n = \Theta + \pi(n - 1)$, see Eq. (5). Note that, for $N \gg 1$, the soliton eigenvalues (11) can also be found within the semi-classical approximation [45],

$$\lambda_n^{(sc)} = i\sqrt{1 - \left[\frac{\pi(n - 1/2)}{L} \right]^2}. \quad (13)$$

For $t = 0$ and $\Theta = 0$, the multi-soliton solution (11)-(12) has real-valued and symmetric in space wavefield,

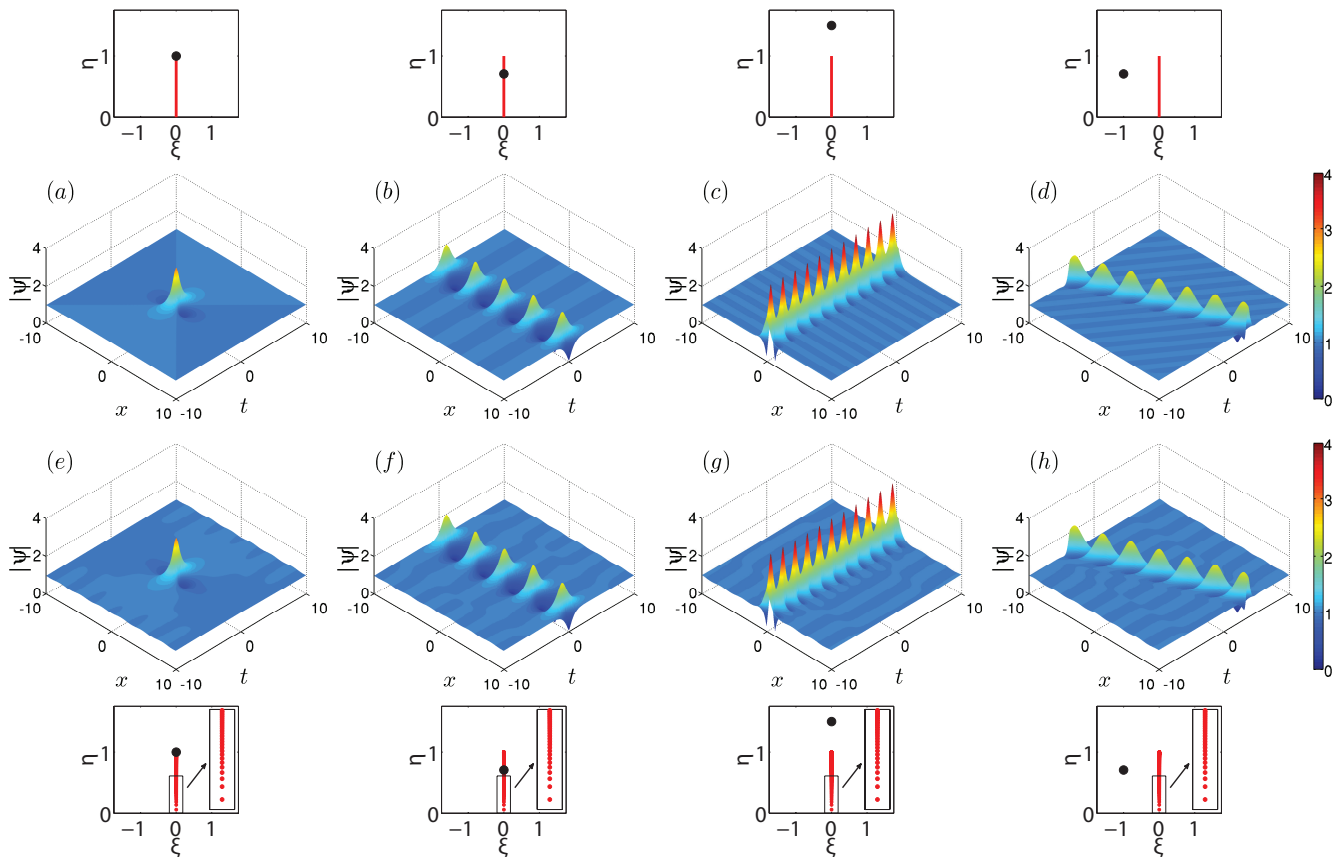


FIG. 4. (*Color on-line*) Space-time representation of (a) the Peregrine breather $\lambda_b = i$, (b) the Akhmediev breather $\lambda_b = i/\sqrt{2}$, (c) the Kuznetsov-Ma breather $\lambda_b = 1.5i$ and (d) the Tajiri-Watanabe breather $\lambda_b = -1 + i/\sqrt{2}$, and (e,f,g,h) their 129-soliton models, respectively. Above and below are shown the corresponding eigenvalue spectra in the upper half of the λ -plane: for exact breather solutions (a,b,c,d) – a combination of the branch cut $[0, i]$ (red line) and soliton λ_b (black circle), while for $(N + 1)$ -soliton models of breathers (e,f,g,h) – a combination of solitons $\{\lambda_n\}$, $n = 1, \dots, N$, from the N -soliton model of the plane wave (11)-(12) (red dots) and soliton λ_b (black circle). Note that, for 128-soliton model of the plane wave, the distance between neighbour eigenvalues is rather small, see the zoom in the corresponding figures.

which models a part of a plane wave $\psi_0^B(x) = 1$ over the interval $|x| \lesssim L/2$; outside this interval, the wavefield is exponentially small. As shown in Fig. 3 for the cases $N = 8$ and 128, in comparison with the plane wave, this N -SS contains residual oscillations due to the absence of nonlinear radiation. In [30], we have demonstrated numerically that in a central region $|x| \leq L_s/2$, which expands to the characteristic width L with increasing N , these residual oscillations vanish by power law with N .

From a mathematical point of view, our construction of solitonic models of breathers assumes the continuity of the DM, meaning that if two potentials ψ_0^B and ψ_N^S are similar, then their dressing with the same soliton $\{\lambda_b, C_b\}$ leads to the similar results. Given that the dressing procedure is local, this is possible when the corresponding wave functions Φ_0^B and Φ_N^S are close to each other in a broad region of space and time. In Appendix D, we verify numerically for some eigenvalues λ that the wave function corresponding to the solitonic model (11)-(12) tends to the wave function for the plane

wave potential with increasing N .

III. SOLITONIC MODELS OF BREATHERS

In the dressing construction of one-breather solutions discussed in Section II B, we replace the plane wave with its N -soliton model (11)-(12). In terms of the schematic illustration shown in Figs. 1-2, this corresponds to replacing the step $n = 0$ in Fig. 2 with the steps from $n = 0$ to N in Fig. 1, during which we build the solitonic model of the plane wave solution. Then, by dressing this solitonic model with the final soliton $\{\lambda_b, C_b\}$, we obtain $(N + 1)$ -soliton models ψ_{N+1}^P , ψ_{N+1}^A , ψ_{N+1}^{KM} and ψ_{N+1}^{TW} for the Peregrine, Akhmediev, Kuznetsov-Ma and Tajiri-Watanabe breathers respectively. In this Section, we compare these models numerically with the analytic solutions ψ^P , ψ^A , ψ^{KM} and ψ^{TW} for the same breathers. For definiteness, we use eigenvalues $\lambda_b = i/\sqrt{2}$, $1.5i$ and $-1 + i/\sqrt{2}$ for the Akhmediev, Kuznetsov-Ma and Tajiri-

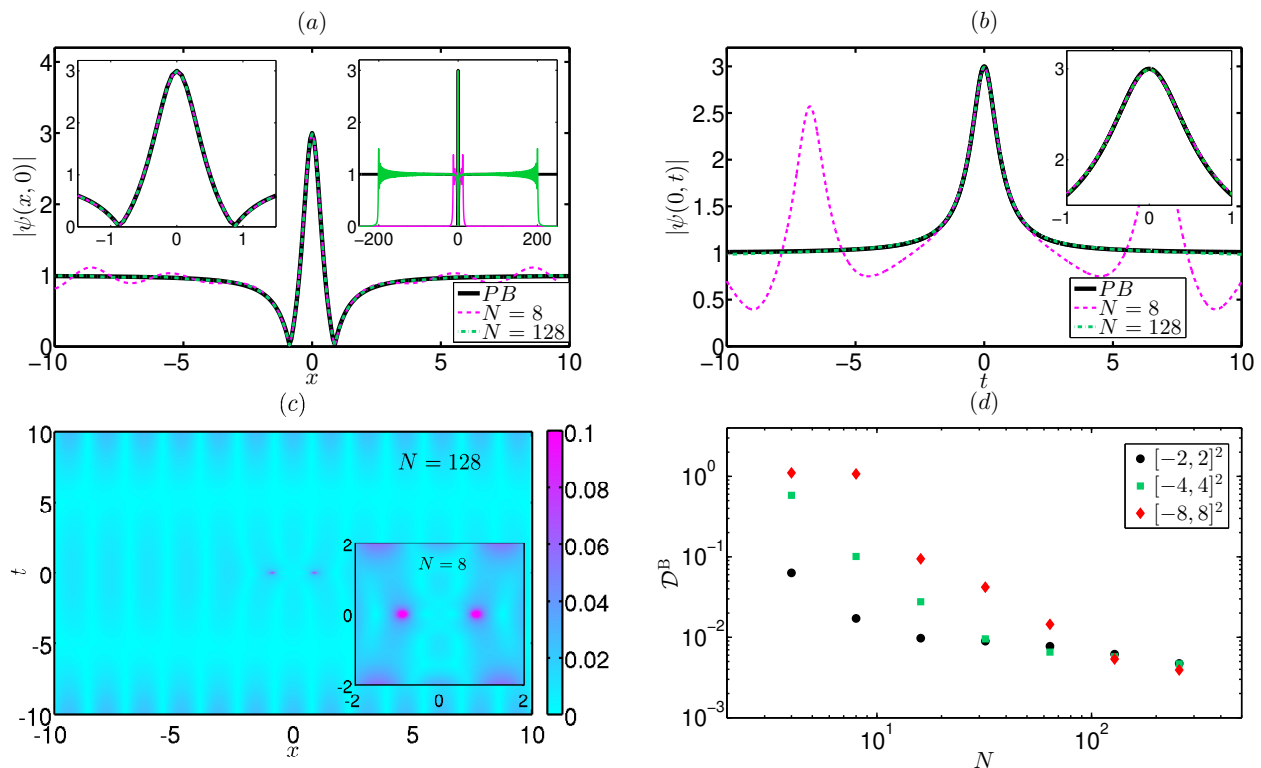


FIG. 5. (*Color on-line*) Peregrine breather (solid black) and its $(N + 1)$ -soliton model (dashed magenta for $N = 8$ and dash-dot green for $N = 128$): (a) space profile $|\psi(x, t_0)|$ at the time $t_0 = 0$ of the maximum elevation, (b) time dependency $|\psi(x_0, t)|$ at the maximum amplitude $x_0 = 0$, and (c) relative deviation (14) in the (x, t) -plane for the $N = 128$ model in the main panel and $N = 8$ model in the inset (note the different scales). Panel (d) shows the integral deviation (15) between the Peregrine breather and its $(N + 1)$ -soliton model versus the number of solitons N used for the modeling of the plane wave, for different regions $(x, t) \in [-\ell, \ell] \times [-\tau, \tau]$ where this deviation is calculated (note the double logarithmic scales). The left inset in panel (a) and inset in panel (b) show zoom near the maximum amplitude, while the right inset in panel (a) demonstrates the solitonic model at large scale. For better visualization, in panel (c), the deviations $d^B(x, t) \geq 0.1$ are indicated with constant deep pink color. Note that panels (a,b,c) are symmetric in space and time.

Watanabe breathers respectively; we have tried other values and came to the same results.

Note that the numerical calculation of multi-soliton wavefields containing a large number of solitons is a highly nontrivial problem due to the large number of arithmetic operations with exponentially small and large numbers. This problem has been solved only recently in [26] with the help of the dressing method and high-precision arithmetics. In the present paper, we use the same scheme to construct multi-soliton solutions at the initial time $t = 0$. To find these solutions at other times, we perform direct numerical simulation of the 1D-NLSE (1) forward and backward in time using the Runge-Kutta fourth-order pseudospectral scheme on adaptive grid, see [58]. An alternative approach would be to repeat the dressing construction for other times; however, our direct simulation provides the same results and takes much less computational resources.

Figure 4 shows the spatiotemporal representation of the analytic breather solutions ψ^P , ψ^A , ψ^{KM} , ψ^{TW} (a,b,c,d) and our $N = 128$ models ψ_{N+1}^P , ψ_{N+1}^A , ψ_{N+1}^{KM} , ψ_{N+1}^{TW} (e,f,g,h), together with the diagrams of the corre-

sponding ZS spectrum. One can see a remarkable correspondence between the breathers and their multi-soliton approximations over a wide region of space and time. In the following, we examine this correspondence in detail for the Peregrine breather, leaving the other breathers for Appendix B.

We start with the spatial profile of the Peregrine breather and its $(N + 1)$ -soliton models for $N = 8$ and $N = 128$, demonstrated in Fig. 5(a) at the time $t = 0$ of the maximum elevation. As illustrated in the inset of the figure, the profile between the two zeros $\psi^P(x, 0) = 0$ is accurately reproduced already by the 9-soliton solution (9-SS). The 129-SS turns out to be practically indistinguishable from the breather over a wide space: in particular, the difference between the two solutions exceeds 0.05 only closer to the edges of the 129-SS, $|\psi_{129}^P(x, 0) - \psi^P(x, 0)| \leq 0.05$ at $|x| < 156$. Comparing the time evolution of the solitonic model and the breather at the point $x = 0$, see Fig. 5(b), we observe that the 9-SS starts to deviate noticeably at $|t| \gtrsim 2$, while the 129-SS model remains close to the breather much longer, $|\psi_{129}^P(0, t) - \psi^P(0, t)| \leq 0.1$ for $|t| \leq 50$.

TABLE I. Integral deviations (15) between breathers and their solitonic models, for the Peregrine (PB) $\lambda_b = i$, Akhmediev (AB) $\lambda_b = i/\sqrt{2}$, Kuznetsov-Ma (KMB) $\lambda_b = 1.5i$ and Tajiri-Watanabe (TWB) $\lambda_b = -1 + i/\sqrt{2}$ breathers.

Breather	$N = 8,$	$N = 128$	
	$[-2, 2]^2$	$[-2, 2]^2$	$[-8, 8]^2$
PB	1.7×10^{-2}	6.2×10^{-3}	5.4×10^{-3}
AB	1.8×10^{-2}	7.9×10^{-3}	5.4×10^{-3}
KMB	2.2×10^{-2}	4.6×10^{-3}	4.7×10^{-3}
TWB	2.0×10^{-2}	6.7×10^{-3}	5.1×10^{-3}

More generally, the deviation of a solitonic model ψ_{N+1}^B from the corresponding breather ψ^B can be measured locally in space and time as

$$d^B(x, t) = \frac{|\psi_{N+1}^B - \psi^B|}{|\psi^B|}. \quad (14)$$

Figure 5(c) shows this deviation for the 129-soliton model in the region $(x, t) \in [-10, 10]^2$ (main figure) and for the 9-soliton model in the region $(x, t) \in [-2, 2]^2$ (inset). For both models, the deviation remains well within 2% for most of the areas demonstrated in the figure, and the maximum relative deviation is observed near the zeros $\psi^P(x, t) = 0$ of the Peregrine breather.

As an integral measure reflecting the deviations, one can consider a quantity

$$D^B = \left[\frac{\int_{-\ell}^{\ell} dx \int_{-\tau}^{\tau} dt |\psi_{N+1}^B - \psi^B|^2}{\int_{-\ell}^{\ell} dx \int_{-\tau}^{\tau} dt |\psi^B|^2} \right]^{1/2}, \quad (15)$$

calculated over the region $(x, t) \in [-\ell, \ell] \times [-\tau, \tau]$. Table I summarizes these integral deviations, demonstrating that the accuracy of our solitonic approximations is very high both in space and in time. Note that deviation (15) depends non-trivially on the number of solitons N used for modeling the plane wave background, as indicated in Fig. 5(d) for three different regions $[-\ell, \ell] \times [-\tau, \tau]$. In particular, as long as the characteristic size of the solitonic model is smaller than the comparison window, $L \lesssim 2\ell$, the deviation stays of unity order; then, it decreases sharply with increasing N , and at larger N the decrease continues according to a less steep law.

It is worth noting that for the solitonic models of the Peregrine and Kuznetsov-Ma breathers, the addition of a single standing soliton to the N -soliton model of the plane wave (11)-(12) perturbs the wavefield of the latter mainly at the center of the solution, $|x| \lesssim 1$. For the Akhmediev breather case, on the contrary, the dressing procedure significantly perturbs the wavefield everywhere in space. For instance, in Fig. 4(b,f), the Akhmediev breather $\lambda_b = i/\sqrt{2}$ at $t = 0$ reaches its maximum $\max|\psi^A| = \sqrt{2} + 1$ on the periodic set of points $x = \pi\sqrt{2}m$, $m \in \mathbb{Z}$, and this behavior is accurately repro-

duced by our solitonic model ψ_{N+1}^A over its entire characteristic width $|x| \lesssim L/2$, see Appendix B for details. The similar situation takes place for the Tajiri-Watanabe breather, since the dressing procedure changes the phase of the background plane wave to the left and to the right from the breather, see Eq. (10). These examples demonstrate the extreme sensitivity of multi-soliton wavefields to changes in the eigenvalue spectrum, when adding just one soliton to a solution, that already contains many more solitons, significantly perturbs the wavefield of the latter everywhere in space.

In Appendix B, we present a detailed comparison between our solitonic models and analytic solutions for the Akhmediev, Kuznetsov-Ma and Tajiri-Watanabe breathers. Also, in Appendix C, we provide the similar results for the higher-order rational and super-regular breathers, which represent specific examples of 2- and 3-breather solutions of the 1D-NLSE.

IV. CONCLUSIONS AND DISCUSSION

We have presented a universal method for the construction of exact multi-soliton solutions which approximate breather dynamics with a very high accuracy over a wide region of space and time. This method consists in replacement of the plane wave background in the dressing construction of the breathers with its solitonic model [30] and then repeating the dressing procedure with exactly the same parameters as used for the construction of the breathers. The resulting solitonic models approximate breathers very well already for $N \sim 10$ solitons, while for $N \sim 100$ solitons they are practically indistinguishable from the breathers over a wide region of space and time. We think that our method can be generalized straightforwardly to multi-breather solutions, breathers on a non-trivial background (e.g., cnoidal waves) and other integrable systems including vector breathers [31–36, 59], making it possible to model the rich dynamics of complex multi-breather solutions [22, 53, 60–63]. We assume that for such a generalization one will only need to find a solitonic model of the breather background.

From a mathematical point of view, our method assumes the continuity of the dressing procedure, when the same dressing of two similar solutions leads to the similar results. Finding the conditions when this continuity is satisfied is an interesting problem for future studies.

We believe that our results have several implications for the studies of rogue waves and, more generally, nonlinear waves. First, as we have noted in the Introduction, the theory of rogue waves needs to be supplemented with localized solutions which evolve locally as breathers. Here we have presented solitonic “skeletons” of such solutions, which (i) can be made of arbitrary characteristic width $L \propto N$ and (ii) become practically indistinguishable from breathers as L increases. Secondly, the modeling of rogue waves with multi-soliton interactions indicates a path to a general explanation for the randomness

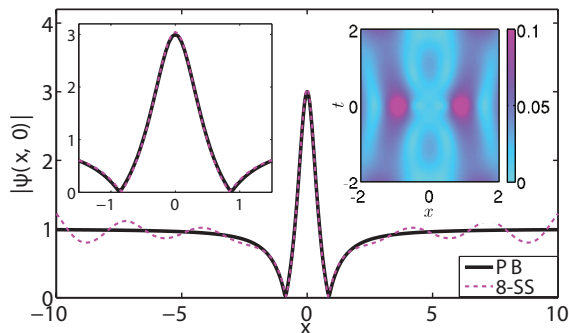


FIG. 6. (Color on-line) Peregrine breather (solid black) and its 8-soliton model (dashed magenta) constructed from the 8-soliton model of the plane wave with two modifications from the procedure discussed in Section III. First, we have used the semi-classical eigenvalues (13) instead of the exact values (11). Second, we have changed the norming constants of the 8-soliton model of the plane wave to $C_n = 1, 1, -1, 1, \dots, -1, 1$, for $n = 1, \dots, 8$, *without the subsequent dressing procedure*. The main panel shows the space profile $|\psi(x, t_0)|$ at the time $t_0 = 0$ of the maximum elevation, the left inset demonstrates zoom near the maximum elevation, and the right inset illustrates the relative deviation (14) in the (x, t) -plane (deviations $d^B(x, t) \geq 0.1$ are indicated with constant deep pink color). The integral deviation (15) in the region $(x, t) \in [-2, 2]^2$ equals 3.0×10^{-2} , that is about twice larger than for the 9-soliton model in Fig. 5.

of rogue waves appearance in terms of the spontaneous synchronization of soliton positions and phases.

Indeed, if a wavefield can be approximated by an exact multi-soliton solution, within which there is a subgroup of solitons corresponding to a certain breather, then one might expect the “appearance” of such breather during the evolution in time. The soliton positions and phases in Eq. (5) evolve as

$$\begin{aligned} x_n(t) &= x_{n0} - 2\xi_n t, \\ \theta_n(t) &= \theta_{n0} + 2(\xi_n^2 + \eta_n^2) t, \end{aligned}$$

where x_{n0} and θ_{n0} are positions and phases at $t = 0$; see e.g. [30] for details. In the general case, the frequencies $2(\xi_n^2 + \eta_n^2)$ are incommensurable. If soliton velocities $-2\xi_n$ are close, i.e., the subgroup travels almost as a bound state, then one might expect the spontaneous synchronization of soliton phases at various moments of time leading to specific synchronizations of soliton norming constants C_n and the appearance of the corresponding breathers. Alternatively, the subgroup may reassemble with other solitons to form another breather.

The exact match of soliton eigenvalues to our solitonic models is not necessary: for instance, in Fig. 6 we have constructed an 8-soliton model of the Peregrine breather with two modifications from the discussed above procedure. First, we have used the semi-classical eigenvalues (13) instead of the exact values (11). Second, we have started from the 8-soliton model of the plane wave

and simply changed its norming constants to $C_n = 1, 1, -1, 1, \dots, -1, 1$, for $n = 1, \dots, 8$, *without the subsequent dressing procedure*. Despite these modifications, the constructed solitonic model still shows a very good correspondence with the breather.

Note, however, that the synchronization conditions inside the subgroup of solitons generating a rogue wave are expected to be strongly influenced by solitons from outside this subgroup. For instance, we observe that adding just one soliton with random parameters to our solitonic models of breathers destroys the similarity with breathers completely. Nevertheless, the correct synchronizations do exist, as evidenced by the recent publication [24], where breather-type rogue waves have been observed in a specific bound-state soliton gas; moreover, the dynamical and statistical properties of these rogue waves matched with those observed in the long-term evolution of the spontaneous modulational instability. Finding the conditions for such synchronizations of soliton parameters represents a challenging problem for future studies.

Finally, our solitonic models may prove useful in explaining the process of soliton fission in nonintegrable systems described at leading order with the focusing 1D-NLSE. Indeed, if the initial wavefield can be approximated by an exact multi-soliton solution, in which most of the solitons are in a bound state, then the influence of nonintegrable perturbations is expected to gradually destroy this state by changing velocities differently for different solitons, thus leading to the fission. Note that soliton fission plays an important role in the supercontinuum generation [64] and formation of optical rogue waves [65]; very recently it has been observed developing from the Peregrine and higher-order rational breathers [28, 29].

Acknowledgements

The authors thank Gennady El for fruitful discussions. This work has been partially supported by the Agence Nationale de la Recherche through the LABEX CEMPI project (ANR-11-LABX-0007), the SOGOOD project (ANR-21-CE30-0061), the Ministry of Higher Education and Research, Hauts de France council and European Regional Development Fund (ERDF) through the Nord-Pas de Calais Regional Research Council and the European Regional Development Fund (ERDF) through the Contrat de Projets Etat-Région (CPER Wavetech). The work of DA was supported by the state assignment of IO RAS, Grant FMWE-2021-0003. DA wishes to thank the Isaac Newton Institute and London Mathematical Society for the financial support on the Solidarity Programme, as well as the Department of Mathematics, Physics and Electrical Engineering at Northumbria University for hospitality. The work of AG was funded by the European Union’s Horizon 2020 research and innovation programme under the Marie Skłodowska-Curie grant No. 101033047. Simulations were performed at the Novosibirsk Supercomputer Center (NSU).

Appendix A: Dressing method

1. The dressing procedure

The dressing method (DM) is based on the representation of a PDE as a compatibility condition of an overdetermined auxiliary linear system – the Lax pair [41, 42]. For the case of the 1D-NLSE,

$$i\psi_t + \frac{1}{2}\psi_{xx} + |\psi|^2\psi = 0, \quad (\text{A1})$$

the Lax pair is known as the Zakharov-Shabat (ZS) system [43] for a two-component vector wave function $\Phi(x, t, \lambda) = (\phi_1, \phi_2)^T$,

$$\Phi_x = \begin{pmatrix} -i\lambda & \psi \\ -\psi^* & i\lambda \end{pmatrix} \Phi, \quad (\text{A2})$$

$$\Phi_t = \begin{pmatrix} -i\lambda^2 + \frac{i}{2}|\psi|^2 & \lambda\psi + \frac{i}{2}\psi_x \\ -\lambda\psi^* + \frac{i}{2}\psi_x^* & i\lambda^2 - \frac{i}{2}|\psi|^2 \end{pmatrix} \Phi, \quad (\text{A3})$$

in which the wavefield ψ of the 1D-NLSE plays the role of a potential. In Eqs. (A2)-(A3), the star stands for the complex conjugate, $\lambda = \xi + i\eta$ is a complex-valued spectral parameter, and Eq. (A1) is obtained as a compatibility condition $\Phi_{xt} = \Phi_{tx}$.

The DM is performed at a specific moment of time which we fix to zero $t = 0$ for simplicity. It starts from an initial background potential $\psi_0(x, t)$ (bare solution) and the corresponding 2×2 matrix solution $\Phi_0(x, t, \lambda)$ of the ZS system (wave function) constructed from two linearly independent solutions of Eqs. (A2)-(A3). At the n -th step of the recursive procedure, the potential $\psi_n(x, t)$ dressed with n solitons is constructed from $\psi_{n-1}(x, t)$ and the corresponding wave function $\Phi_{n-1}(x, t, \lambda)$ as

$$\psi_n(x, t) = \psi_{n-1}(x, t) + 2i(\lambda_n - \lambda_n^*) \frac{q_{n1}^* q_{n2}}{|\mathbf{q}_n|^2}. \quad (\text{A4})$$

In this relation, vector $\mathbf{q}_n = (q_{n1}, q_{n2})^T$ is determined via Φ_{n-1} , the soliton eigenvalue λ_n , and an arbitrary constant $C_n \in \mathbb{C} \setminus \{0\}$ which we call the norming constant,

$$\mathbf{q}_n(x, t) = [\Phi_{n-1}(x, t, \lambda_n^*)]^* \cdot \begin{pmatrix} C_n^{-1/2} \\ C_n^{1/2} \end{pmatrix}. \quad (\text{A5})$$

The corresponding wave function $\Phi_n(x, t, \lambda)$ is calculated using the dressing matrix $\sigma^{(n)}(x, t, \lambda)$,

$$\Phi_n(x, t, \lambda) = \sigma^{(n)}(x, t, \lambda) \cdot \Phi_{n-1}(x, t, \lambda), \quad (\text{A6})$$

$$\sigma_{ml}^{(n)}(x, t, \lambda) = \delta_{ml} + \frac{\lambda_n - \lambda_n^*}{\lambda - \lambda_n} \frac{q_{nm}^* q_{nl}}{|\mathbf{q}_n|^2}, \quad (\text{A7})$$

where $m, l = 1, 2$ and δ_{ml} is the Kronecker delta. The outcome of the dressing by N solitons can be written via

the ratio of two determinants,

$$\psi_N(x, t) = \psi_0 - 2i \frac{\det \mathbf{P}}{\det \mathbf{Q}}, \quad Q_{kj} = \frac{(\tilde{\mathbf{q}}_k \cdot \tilde{\mathbf{q}}_j^*)}{\lambda_k - \lambda_j^*},$$

$$\mathbf{P} = \begin{pmatrix} 0 & \tilde{q}_{12} & \cdots & \tilde{q}_{N2} \\ \tilde{q}_{11}^* & & & \\ \vdots & & \mathbf{Q}^T & \\ \tilde{q}_{N1}^* & & & \end{pmatrix}, \quad (\text{A8})$$

where the new vectors $\tilde{\mathbf{q}}_n = (\tilde{q}_{n1}, \tilde{q}_{n2})^T$ depend on the initial matrix Φ_0 , and we discuss them separately for the multi-soliton and multi-breather cases.

2. Multi-soliton and multi-breather solutions

An exact N -soliton potential is constructed from the zero background $\psi_0^S(x, t) = 0$ and the corresponding wave function

$$\Phi_0^S(x, t, \lambda) = \begin{pmatrix} e^{-i\lambda x - i\lambda^2 t} & 0 \\ 0 & e^{i\lambda x + i\lambda^2 t} \end{pmatrix}, \quad (\text{A9})$$

with the outcome written as

$$\psi_N^S(x, t) = -2i \frac{\det \mathbf{P}}{\det \mathbf{Q}}. \quad (\text{A10})$$

The matrices \mathbf{P} and \mathbf{Q} are defined via vectors

$$\tilde{\mathbf{q}}_n(x, t) = \begin{pmatrix} \tilde{q}_{n1} \\ \tilde{q}_{n2} \end{pmatrix} = \begin{pmatrix} C_n^{-1/2} e^{i\lambda_n x + i\lambda_n^2 t} \\ C_n^{1/2} e^{-i\lambda_n x - i\lambda_n^2 t} \end{pmatrix}. \quad (\text{A11})$$

If one parametrizes the norming constants C_n via the soliton position $x_n \in \mathbb{R}$ and phase $\theta_n \in \mathbb{R}$ as

$$C_n = \exp[i\pi + 2i\lambda_n x_n + i\theta_n], \quad (\text{A12})$$

then the one-soliton potential takes the following form,

$$\psi_1^S(x, t) = a_1 \frac{\exp[iv_1(x - x_1) + \frac{i(a_1^2 - v_1^2)t}{2} + i\theta_1]}{\cosh a_1(x - v_1 t - x_1)},$$

where $a_1 = 2\eta_1$ and $v_1 = -2\xi_1$ are the soliton amplitude and velocity. Note that parametrization (A12) serves only for a convenient and physically intuitive representation of multi-soliton solutions, and that x_n and θ_n coincide with the observed in the physical space position and phase of a soliton only for one-soliton potential. In presence of other solitons or dispersive waves, the observed position and phase may differ considerably from these parameters.

An exact N -breather potential is constructed from the plane wave background $\psi_0^B(x, t) = e^{it + i\Theta}$, where $\Theta \in \mathbb{R}$ is the initial phase, and the corresponding wave function,

$$\Phi_0^B(x, t, \lambda) = \begin{pmatrix} e^{\frac{i}{2}t - \phi} & p e^{i\Theta + \frac{i}{2}t + \phi} \\ p e^{-i\Theta - \frac{i}{2}t - \phi} & e^{-\frac{i}{2}t + \phi} \end{pmatrix}, \quad (\text{A13})$$

$$\phi = i\zeta(x + \lambda t), \quad p = i(\lambda - \zeta), \quad \zeta = \sqrt{1 + \lambda^2}.$$

Note that, as is usually done in the breather theory, for the function $\zeta(\lambda)$ we use the branch cut $[-i, i]$, choosing the Riemann sheet such that $\text{Im} \zeta > 0$ at $\text{Im} \lambda > 0$. This choice differs from the branch cut $i(-\infty, -1] \cup i[1, \infty)$ implied in software compilers. In the outcome of the dressing procedure, the plane wave $e^{it+i\Theta}$ can be extracted as a common factor,

$$\psi_N^B(x, t) = e^{it+i\Theta} \left(1 - 2i \frac{\det \mathbf{P}}{\det \mathbf{Q}} \right), \quad (\text{A14})$$

while the matrices \mathbf{P} and \mathbf{Q} are defined via vectors

$$\begin{aligned} \tilde{\mathbf{q}}_n(x, t) = & \quad (\text{A15}) \\ & \begin{pmatrix} C_n^{-1/2} e^{i\frac{\Theta}{2}} e^{\phi_n} - C_n^{1/2} e^{-i\frac{\Theta}{2}} p_n e^{-\phi_n} \\ -C_n^{-1/2} e^{i\frac{\Theta}{2}} p_n e^{\phi_n} + C_n^{1/2} e^{-i\frac{\Theta}{2}} e^{-\phi_n} \end{pmatrix}, \\ \phi_n = & i\zeta_n(x + \lambda_n t), \quad p_n = i(\lambda_n - \zeta_n), \quad \zeta_n = \zeta(\lambda_n). \end{aligned}$$

In particular, a one-breather solution – that is, the general Tajiri-Watanabe breather [16, 53] – has the following representation via vector $\tilde{\mathbf{q}}_1$,

$$\psi_1^B(x, t) = e^{it+i\Theta} \left(1 - 4\eta_1 \frac{\tilde{q}_{11}^* \tilde{q}_{12}}{|\tilde{q}_{11}|^2 + |\tilde{q}_{12}|^2} \right). \quad (\text{A16})$$

3. Fundamental breather solutions

Depending on the choice of the soliton eigenvalue relative to the branch cut $[-i, i]$, a general one-breather potential represents one of the four different cases (i) $\lambda_b = i$, (ii) $\lambda_b = i\eta_b$ with $\eta_b < 1$, (iii) $\lambda_b = i\eta_b$ with $\eta_b > 1$ and (iv) $\text{Re} \lambda_b \neq 0$, corresponding to the Peregrine, Akhmediev, Kuznetsov-Ma and Tajiri-Watanabe breathers respectively. As in the main paper, we have changed the subscript of the eigenvalue λ_b and the corresponding norming constant C_b to reflect that this soliton is used for dressing the plane wave. In the following, we use different parametrizations of the norming constant C_b for different breathers. These parametrizations are needed to represent the corresponding solutions in a convenient and physically intuitive form, and also to place the breathers at a given position in space and/or time.

The Akhmediev breather is obtained by dressing a bare solution $\psi_0^B = e^{it+i\Theta}$ with soliton $\lambda_b = i\eta_b$, $\eta_b < 1$. If one parameterizes the norming constant as

$$C_b^A = \exp [i(\pi + \Theta) + \Omega_A t_0 + i\theta_0], \quad (\text{A17})$$

then, this breather takes the following form,

$$\begin{aligned} \psi^A(x, t) = & e^{it+i\Theta+i\pi} \times \quad (\text{A18}) \\ & \times \left(1 - \frac{2\kappa^2 \cosh[\Omega_A(t-t_0)] + i\Omega_A \sinh[\Omega_A(t-t_0)]}{\cosh[\Omega_A(t-t_0)] - \eta_b \cos[2\kappa x + \theta_0]} \right), \end{aligned}$$

where $\kappa = \sqrt{1 - \eta_b^2}$ and $\Omega_A = 2\eta_b \kappa$, while $t_0 \in \mathbb{R}$ and $\theta_0 \in [0, 2\pi)$ correspond to the time shift and space phase shift respectively.

The Kuznetsov-Ma breather is constructed by dressing with soliton $\lambda_b = i\eta_b$, $\eta_b > 1$. With parametrization

$$C_b^{\text{KM}} = \exp [i(\pi + \Theta) - 2\nu x_0 + i\theta_0], \quad (\text{A19})$$

this solution can be written as

$$\begin{aligned} \psi^{\text{KM}}(x, t) = & e^{it+i\Theta+i\pi} \times \quad (\text{A20}) \\ & \times \left(1 - \frac{2\nu^2 \cos[\Omega_K t + \theta_0] + i\Omega_K \sin[\Omega_K t + \theta_0]}{\eta_b \cosh[2\nu(x-x_0)] - \cos[\Omega_K t + \theta_0]} \right), \end{aligned}$$

where $\nu = \sqrt{\eta_b^2 - 1}$ and $\Omega_K = 2\eta_b \nu$, while $x_0 \in \mathbb{R}$ and $\theta_0 \in [0, 2\pi)$ represent the space shift and time phase shift respectively.

The Peregrine breather is obtained from the Kuznetsov-Ma solution in the limit $\epsilon = (\eta_b - 1) \rightarrow 0^+$, corresponding to the dressing with soliton $\lambda_b = i$. Expanding Eq. (A20) in Taylor series with respect to ϵ for $|x - x_0| \ll (8\epsilon)^{-1/2}$ and $|t| \ll (8\epsilon)^{-1/2}$, and using the following parametrization of the norming constant,

$$C_b^P = \exp [i(\pi + \Theta) - \sqrt{8\epsilon}(x_0 + it_0)], \quad (\text{A21})$$

we arrive to the Kuznetsov-Ma breather that behaves locally as the Peregrine breather,

$$\begin{aligned} \psi^P(x, t) = & e^{it+i\Theta+i\pi} \times \quad (\text{A22}) \\ & \times \left(1 - \frac{4(1 + 2i[t-t_0])}{1 + 4[x-x_0]^2 + 4[t-t_0]^2} \right). \end{aligned}$$

Here $x_0 \in \mathbb{R}$ and $t_0 \in \mathbb{R}$ are the position and time shifts respectively. Note that formally, at $\epsilon = 0$, there is only one allowed value of the norming constant $C_b = e^{i\pi+i\Theta}$, which corresponds to the Peregrine breather (A22) for all possible x_0 and t_0 . Any other value of C_b results in the plane wave solution $\psi^P = e^{it+i\Theta+i\pi}$ describing the Peregrine breather located at infinity. The specific values of x_0 and t_0 are determined by how the norming constant (A21) tends to $e^{i\pi+i\Theta}$ in the limit $\epsilon \rightarrow 0^+$.

The Tajiri-Watanabe breather corresponds to a general case when the soliton eigenvalue λ_b has nonzero real and imaginary parts, so that we use Eq. (A16) without simplifications. This solution describes a coherent wave group on the background of the plane wave, which moves with a constant velocity $V_{\text{TW}} = -\text{Im}[\lambda_b \zeta_b] / \text{Im} \zeta_b$ in space and oscillates with a frequency $\Omega_{\text{TW}} = 4 \text{Re}[\lambda_b \zeta_b] - 4 V_{\text{TW}} \text{Re} \zeta_b$ in time; here $\zeta_b = \zeta(\lambda_b)$. The following parametrization of the norming constant,

$$C_b^{\text{TW}} = \exp [i(\pi + \Theta) + 2i\zeta_b x_0 + i\theta_0], \quad (\text{A23})$$

allows one to find the position x_0 and phase θ_0 of the breather at the initial time $t = 0$.

In terms of evolution of the amplitude $|\psi|$, the Tajiri-Watanabe breather represents a localized perturbation on the background of the plane wave, see e.g. Fig. 4(d) in the main paper. However, it has different phases of this background to the left and to the right of itself,

$$\lim_{x \rightarrow \pm\infty} \frac{\psi^{\text{TW}}(x, t)}{e^{it+i\Theta}} = \exp \left(\pm 2i \arg[\zeta_b + \lambda_b] \right), \quad (\text{A24})$$

meaning that the corresponding perturbation of the wavefield ψ is not localized. Eq. (A24) is obtained by taking the limits $x \rightarrow \pm\infty$ in Eq. (A16) and is valid for any localized breather solution of the 1D-NLSE. Note that, in the main paper, this equation is written in a modified form (10), which can be understood using the Zhukovsky transform to the variables $\alpha \in [0, 2\pi)$ and $R \in [0, \infty)$,

$$\lambda = \frac{i}{2} \left(R e^{i\alpha} + \frac{e^{-i\alpha}}{R} \right), \quad \zeta = \frac{i}{2} \left(R e^{i\alpha} - \frac{e^{-i\alpha}}{R} \right) \quad (\text{A25})$$

see e.g. [39] for the application of this transform in the theory of breathers. In the new variables $\arg[\zeta_b + \lambda_b] = \alpha_b + \pi/2$, and the phase shift by $\pi/2$ can be moved to the denominator of the left-hand side of Eq. (A24), leading to Eq. (10) of the main paper,

$$\lim_{x \rightarrow \pm\infty} \frac{\psi^{\text{TW}}(x, t)}{e^{it+i\Theta+i\pi}} = \exp(\pm 2i\alpha_b). \quad (\text{A26})$$

In the general case of an N -breather potential containing only the localized Peregrine, Kuznetsov-Ma and Tajiri-Watanabe breathers, the phase of the plane wave to the left and to the right can be found as a multiplication of the factors (A26),

$$\lim_{x \rightarrow \pm\infty} \frac{\psi_N^{\text{B}}(x, t)}{e^{it+i\Theta+iN\pi}} = \exp \left[\pm 2i \sum_{n=1}^N \alpha_n \right]. \quad (\text{A27})$$

In some cases, e.g., for a pair of super-regular breathers, one can achieve the same phase in the limits $x \rightarrow \pm\infty$, that corresponds to a localized perturbation of the plane wave [62]. As follows from Eq. (A27), each new breather changes the phase of the plane wave background by π .

Appendix B: Solitonic models of one-breather solutions

In the main paper, we have presented a detailed numerical comparison between the Peregrine breather ψ^{P} and its $(N+1)$ -soliton model ψ_{N+1}^{P} . Here we provide the similar results for the Akhmediev ψ^{A} , Kuznetsov-Ma ψ^{KM} and Tajiri-Watanabe ψ^{TW} breathers versus their solitonic models ψ_{N+1}^{A} , ψ_{N+1}^{KM} and ψ_{N+1}^{TW} respectively. For definiteness, we use parameters $\Theta = \pi$ and $C_b = 1$ for the dressing construction, as they correspond to the canonical form of the breathers given in the main paper. As for the eigenvalues, we set $\lambda_b = i/\sqrt{2}$, $1.5i$ and $-1 + i/\sqrt{2}$ for the Akhmediev, Kuznetsov-Ma and Tajiri-Watanabe breathers respectively; we have tried other values and came to the same results.

Figure 7(a,d,g) shows the spatial profiles of the breathers at the time $t = 0$ of their maximum elevation versus the corresponding $(N+1)$ -soliton models for $N = 8$ and $N = 128$. One can see that profiles between the two amplitude minima closest to the coordinate origin $x = 0$ are accurately reproduced already by the 9-soliton solutions (9-SS), while the 129-SS are practically

indistinguishable from the breathers over a wide space. Comparing the time evolution of the breathers and their solitonic models at $x = 0$ in Fig. 7(b,e,h), we observe that the 9-SS deviate noticeably at $|t| \gtrsim 2$, while the 129-SS remain close to the breathers for a much longer time.

The relative deviation between the breathers ψ^{B} and their solitonic models ψ_{N+1}^{B} in space and time,

$$d^{\text{B}}(x, t) = \frac{|\psi_{N+1}^{\text{B}} - \psi^{\text{B}}|}{|\psi^{\text{B}}|}, \quad (\text{B1})$$

is shown in Fig. 7(c,f,i): for the 129-soliton models in the region $(x, t) \in [-10, 10]^2$ – in the main figures, and for the 9-SS in the region $(x, t) \in [-2, 2]^2$ – in the insets. For all cases, the deviation (B1) remains within 2% for most of the areas demonstrated in the figures, and the maximum relative deviation is observed near the local minima $\min |\psi^{\text{B}}(x, t)|$. The integral deviation of the solitonic models from the breathers,

$$D^{\text{B}} = \left[\frac{\int_{-\ell}^{\ell} dx \int_{-\tau}^{\tau} dt |\psi_{N+1}^{\text{B}} - \psi^{\text{B}}|^2}{\int_{-\ell}^{\ell} dx \int_{-\tau}^{\tau} dt |\psi^{\text{B}}|^2} \right]^{1/2}, \quad (\text{B2})$$

is provided in Table I of the main paper; it is about 2% for the 9-soliton models in the region $[-2, 2]^2$ and about 0.6% for the 129-SS in the region $[-8, 8]^2$.

As we have noted in the main paper, for the case of the Akhmediev breather, the dressing by a single soliton of the solitonic model of the plane wave changes the wavefield of the latter significantly everywhere in space. In particular, at $t = 0$, the Akhmediev breather $\lambda_b = i/\sqrt{2}$ reaches its maximum $\max |\psi^{\text{A}}| = \sqrt{2} + 1$ on the periodic set of points $x = \pi\sqrt{2}m$, $m \in \mathbb{Z}$, and this behavior is accurately reproduced by our solitonic model over its entire characteristic width $|x| \lesssim L/2$; see the right inset in Fig. 7(a). The similar situation takes place for the Tajiri-Watanabe breather, for which the dressing procedure changes the phase of the plane wave background to the left and to the right from the breather; see Eq. (A26) and the left inset in Fig. 7(g).

Appendix C: Higher-order rational and super-regular breathers

In this Section, we generalize our results for multi-breather solutions, namely, the higher-order rational [37] and super-regular [38–40] breathers.

Higher-order rational breathers are constructed when the (bare) plane wave $\psi_0^{\text{B}} = e^{it+i\Theta}$ is repeatedly dressed with the same soliton $\lambda_b = i$ using the same norming constant C_b . In particular, the second-order rational breather is obtained by double dressing, the third-order by triple dressing, and so on. Numerically, the dressing scheme discussed in Section A 1 cannot be applied in this way due to the division by zero in Eq. (A5) during the repeated dressings, see Eqs. (A6)-(A7), while analytically this difficulty can be overcome by applying the

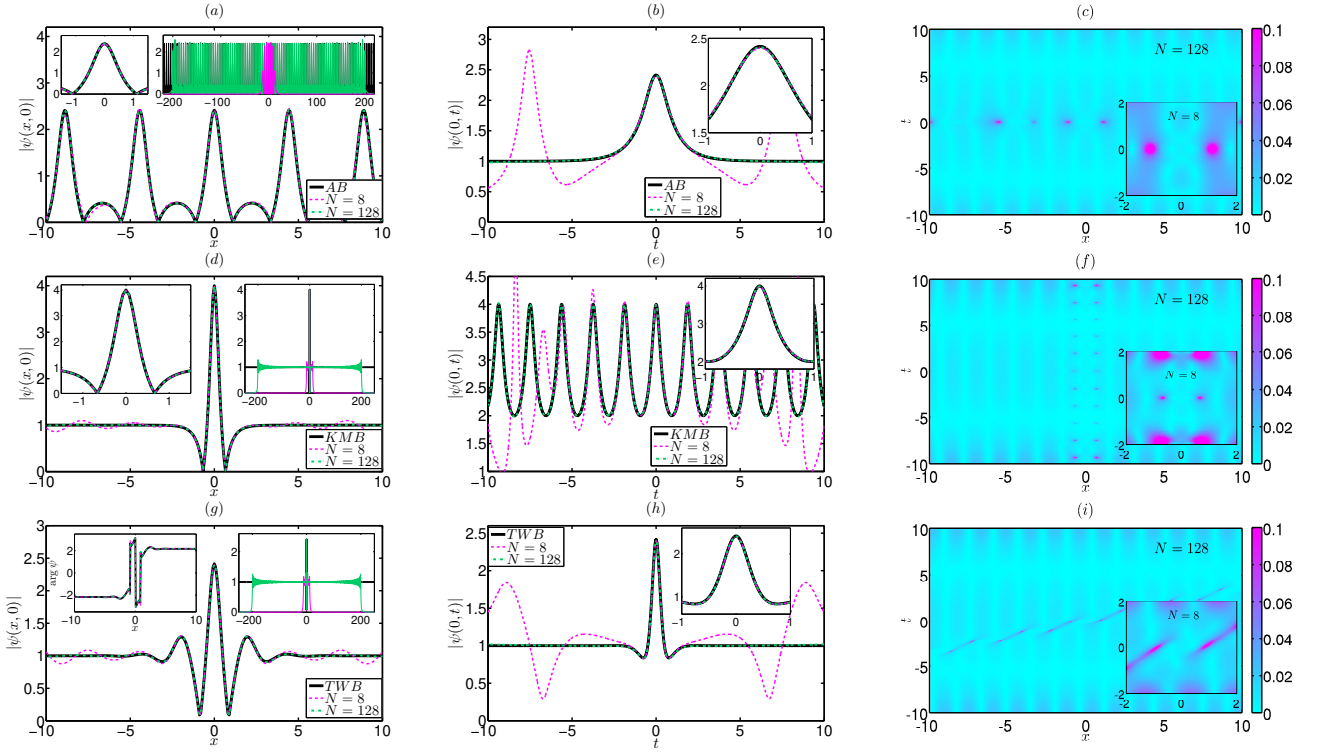


FIG. 7. (Color on-line) Comparison of the Akhmediev $\lambda_b = i/\sqrt{2}$ (a,b,c), Kuznetsov-Ma $\lambda_b = 1.5i$ (d,e,f) and Tajiri-Watanabe $\lambda_b = -1 + i/\sqrt{2}$ (g,h,i) breathers with their $(N + 1)$ -soliton models. The analytic solutions are shown with solid black lines, while the 9- and 129-soliton models are indicated with dashed magenta and dash-dot green. Panels (a,d,g) demonstrate space profiles $|\psi(x, t_0)|$ at the time $t_0 = 0$ of the maximum elevation, panels (b,e,h) show the time dependency $|\psi(x_0, t)|$ at the coordinate origin $x_0 = 0$, and panels (c,f,i) illustrate the relative deviation (B1) in the (x, t) -plane for the 129-soliton models in the main panels and the 9-SS in the insets (note the different scales). The left insets in panels (a,d) and insets in panels (b,e,h) show zoom near the maximum elevation, the left inset in panel (g) illustrates the phase $\arg \psi$ of the Tajiri-Watanabe breather and its solitonic models, and the right insets in panels (a,d,g) demonstrate solitonic models at large scales. For better visualization, in panels (c,f,i), the deviations $d^B(x, t) \geq 0.1$ are shown with constant deep pink color.

TABLE II. Integral deviations (B2) between breathers and their solitonic models, for the rational breather of the 2nd order (RB₂) $\lambda_{b1,b2} = i$, rational breather of the 3rd order (RB₃) $\lambda_{b1,b2,b3} = i$, and a pair of super-regular breathers (SRB) $\lambda_{b1,b2} = \pm 0.15 + i/\sqrt{2}$.

Breather	$N = 8$, [-2, 2] ²	$N = 128$	
		[-2, 2] ²	[-8, 8] ²
RB ₂	1.1×10^{-2}	4.6×10^{-3}	6.6×10^{-3}
RB ₃	9.4×10^{-3}	4.0×10^{-3}	5.9×10^{-3}
SRB	3.2×10^{-2}	7.7×10^{-3}	5.7×10^{-3}

L'Hospital's rule. For this reason, we build solitonic models of the higher-order rational breathers by using slightly different solitons $\lambda_{bj} = i(1 + j \Delta\eta)$ with the same norming constants C_{bj} , where $\Delta\eta = 10^{-6}$, $j = 0, \dots, M - 1$, and M is the order of the breather. We use parameters $\Theta = M\pi$ and $C_{bj} = (-1)^{M-1}$, for which the breathers take their canonical form and represent localized rational perturbations of the plane wave e^{it} leading to the maxi-

imum amplitude $\max |\psi^{RM}(x, t)| = 2M + 1$ at the point $(0, 0)$. We do not provide exact analytic relations for the breathers as they are too cumbersome, and instead refer the reader to [37] where they were first found.

Super-regular breathers are two-breather solutions constructed by dressing with solitons $\lambda_{b1,b2} = \pm \xi_b + i\eta_b$ with $|\xi_b| \ll 1$ and $\eta_b < 1$. For specific combinations of the norming constants $C_{b1,b2}$, these solutions represent localized perturbations of the plane wave with characteristic amplitude $\propto |\xi_b|$ and width $\propto |\xi_b|^{-1}$, which lead to the same phases of the plane wave background in the limits $x \rightarrow \pm\infty$; see Eq. (A27). We build their solitonic models using the parameters $\Theta = 0$ and $C_{b1,b2} = -i$, for which the breathers represent small localized perturbations of the plane wave e^{it} , and compare the models with the exact solutions first found in [38]. Note that a more general choice of the eigenvalues is possible [39, 62] with non-symmetric spatial profiles of the wavefields. For definiteness, we use $\lambda_{b1,b2} = \pm 0.15 + i/\sqrt{2}$; we have tried other values and came to the same results.

Figure 8 shows a comparison of our solitonic models for $N = 8$ and 128 with the exact breather solutions for the

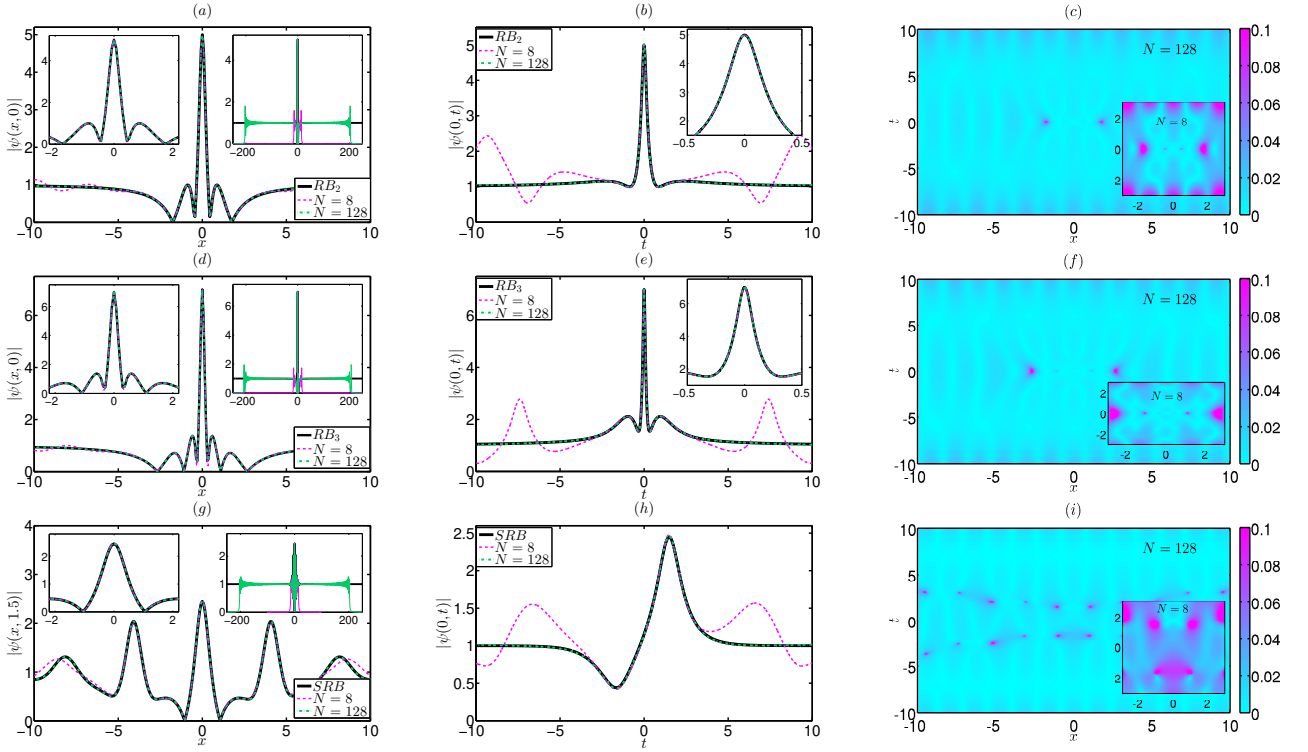


FIG. 8. (Color on-line) Same as in Fig. 7 for the rational breather of the 2nd order $\lambda_{b1,b2} = i$ (a,b,c), rational breather of the 3rd order $\lambda_{b1,b2,b3} = i$ (d,e,f), and a pair of super-regular breathers $\lambda_{b1,b2} = \pm 0.15 + i/\sqrt{2}$ (g,h,i). The maximum elevation for the super-regular breathers is achieved at $t_0 \approx 1.5$, so that this moment of time is shown in panel (g) instead of $t = 0$.

second-order rational (a,b,c), third-order rational (d,e,f), and super-regular (g,h,i) breathers. Here N is the number of solitons used for the modeling of the plane wave background, so that our solitonic models contain 10-11 and 130-131 solitons. One can see that the results of this comparison are very similar to those discussed in the main paper and in Section B. In particular, the spatial profiles of the breathers at the time of their maximum elevation are accurately reproduced already by the $N = 8$ models between the two adjacent local minima, while the $N = 128$ models are practically indistinguishable from the breathers over a wide region of space and time. The integral deviations (B2) between the models and the breathers given in Table II equal to 1-3% for the $N = 8$ models in the region $[-2, 2]^2$ and about 0.6% for the $N = 128$ models in the region $[-8, 8]^2$.

We conclude that our method allows one to reproduce multi-breather dynamics over a wide region of space and time with a very high accuracy using exact multi-soliton solutions.

Appendix D: Wave function for the solitonic model of the plane wave

As follows from Eqs. (A4)-(A7), the dressed potential and wave function ψ_n and Φ_n depend on ψ_{n-1} and Φ_{n-1} taken at the same point (x, t) , so that the dressing proce-

dure is local. Also, if two bare potentials ψ_0 and $\tilde{\psi}_0$ are similar, and the corresponding wave functions Φ_0 and $\tilde{\Phi}_0$ are similar as well, then their identical dressing will lead to the similar potentials ψ_1 and $\tilde{\psi}_1$, meaning the continuity of the dressing procedure. This property may underlie our results on the similarity between breather solutions and our solitonic models – if only the wave functions Φ_0^B and Φ_N^S corresponding to the plane wave and its N -soliton model are similar. Here we verify this similarity numerically by comparing wave function (A13) with that of the solitonic model of the plane wave.

Note that wave function depends on three variables x , t and λ . We are unable to perform a systematic comparison in this three-dimensional space, and instead fix $t = 0$ and $\lambda = 1.5i$, and then compare the spatial behavior over the x -coordinate. We have tried a number of other combinations of times t (not large) and eigenvalues λ (both $\text{Im } \lambda \geq 1$ and $\text{Im } \lambda < 1$), and came to the similar results. Also note that, in the dressing procedure, the wave function of the previous step is evaluated at the complex-conjugate point λ^* , see Eq. (A5). For this reason, in the following, we perform comparison between wave functions $\Phi_0^B(x, t, \lambda^*)$ and $\Phi_N^S(x, t, \lambda^*)$.

If λ is not from the discrete spectrum of the solitonic model of the plane wave, see Eq. (11) in the main paper, then both $\Phi_0^B(x, t, \lambda^*)$ and $\Phi_N^S(x, t, \lambda^*)$ are unbounded and exhibit exponential behavior in the x -space, see Eq. (A13). For visual comparison, we multiply the

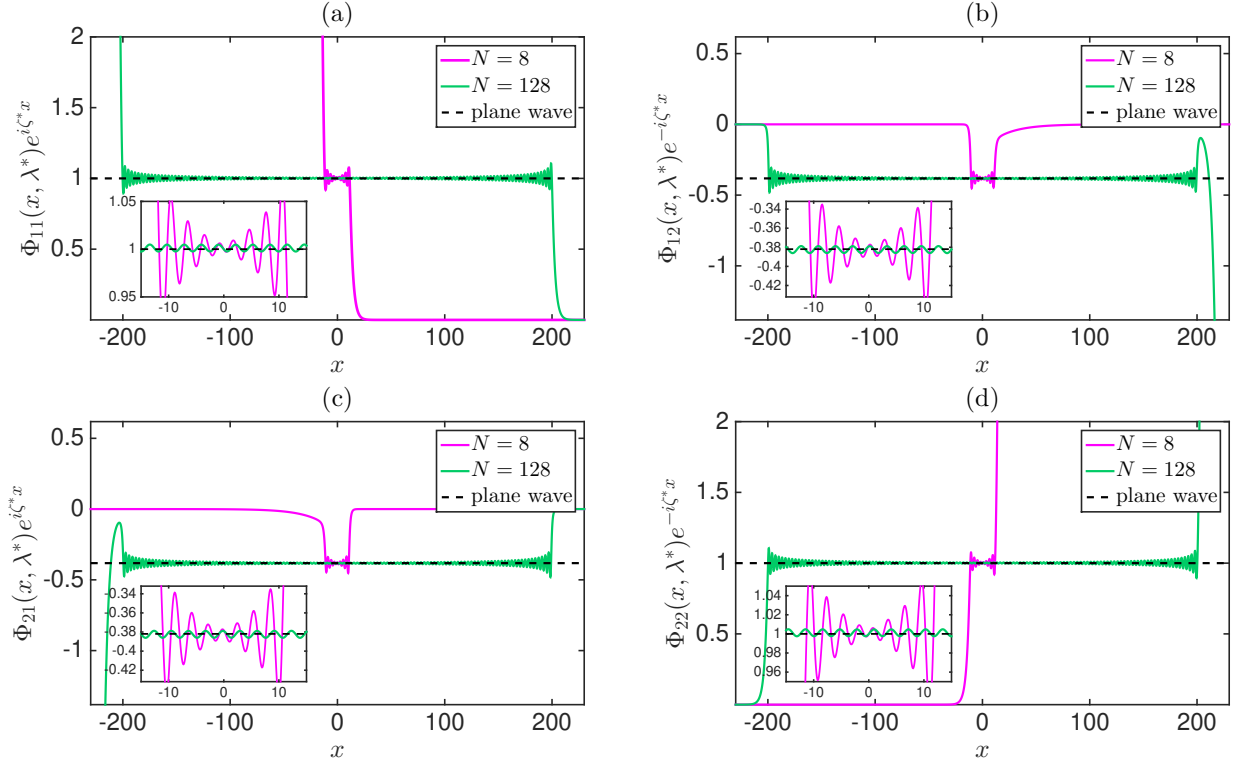


FIG. 9. (*Color on-line*) Spatial behavior of the elements of wave functions $\Phi_0^B(x, t, \lambda^*)$ (dashed black) and $\Phi_N^S(x, t, \lambda^*)$ (magenta for $N = 8$ and green for $N = 128$) at $t = 0$ and $\lambda = 1.5i$: (a) Φ_{11} , (b) Φ_{12} , (c) Φ_{21} and (d) Φ_{22} . As in the main paper, we use $\Theta = \pi$ for the plane wave and its solitonic model. Wave functions are normalized so that their first element equals unity at $x = 0$. Also, for visual comparison, we multiply the elements either by $e^{i\zeta^*x}$, or by $e^{-i\zeta^*x}$ to compensate the exponential behavior. We demonstrate only the real part of the wave functions, since the imaginary part is identically zero at $t = 0$.

elements of these matrices either by $e^{i\zeta^*x}$, or by $e^{-i\zeta^*x}$, compensating the leading exponent. Additionally, the ZS system is linear, so that different solutions may have different normalizations. For this reason, before comparison, we normalize wave functions by multiplying all four matrix elements by the same constant so that the first matrix element becomes unity at $x = 0$, $\Phi_{11}(0, t, \lambda^*) = 1$. As follows from Eqs. (A4)-(A5) and (A7), such a change of normalization does not affect the dressing procedure.

Figure 9 shows elements of wave function (A13) (dashed black lines) in comparison with the corresponding elements of Φ_N^S for $N = 8$ (magenta) and $N = 128$ (green). One can see a very good agreement over the entire characteristic width $|x| \lesssim L/2$, $L = \pi(N - 1/4)$,

of the solitonic model of the plane wave. Very similarly to this model (compare with Fig. 3 in the main paper), Φ_N^S oscillates around the exact solution (A13), and these oscillations decrease with the growing number of solitons N .

This comparison confirms that our solitonic model of the Kuznetsov-Ma breather $\lambda_b = 1.5i$ is similar to the exact breather due to (i) the locality and continuity of the dressing procedure, and (ii) the fact that the wave function corresponding to the solitonic model of the plane wave is similar to the exact solution (A13) at $\lambda_b^* = -1.5i$. We have come to the same result for a number of other eigenvalues, including those corresponding to the Akhmediev breather.

-
- [1] C. Kharif and E. Pelinovsky, Physical mechanisms of the rogue wave phenomenon, *Eur. J. Mech.-B/Fluids* **22**, 603 (2003).
 [2] K. Dysthe, H. E. Krogstad, and P. Muller, Oceanic rogue waves, *Annu. Rev. Fluid Mech.* **40**, 287 (2008).
 [3] M. Onorato, S. Residori, U. Bortolozzo, A. Montina, and F. T. Arecchi, Rogue waves and their generating mechanisms in different physical contexts, *Phys. Rep.* **528**, 47

- (2013).
 [4] J. M. Dudley, G. Genty, A. Mussot, A. Chabchoub, and F. Dias, Rogue waves and analogies in optics and oceanography, *Nat. Rev. Phys.* **1**, 675 (2019).
 [5] K. B. Dysthe and K. Trulsen, Note on breather type solutions of the NLS as models for freak-waves, *Phys. Scr.* **1999**, 48 (1999).
 [6] A. R. Osborne, M. Onorato, and M. Serio, The nonlinear

- dynamics of rogue waves and holes in deep-water gravity wave trains, *Phys. Lett. A* **275**, 386 (2000).
- [7] A. Osborne, *Nonlinear Ocean Waves and the Inverse Scattering Transform* (Academic Press, 2010).
- [8] V. I. Shrira and V. V. Geogjaev, What makes the peregrine soliton so special as a prototype of freak waves?, *J. Eng. Math.* **67**, 11 (2010).
- [9] Y. S. Kivshar and G. Agrawal, *Optical solitons: from fibers to photonic crystals* (Academic press, London, 2003).
- [10] C. Kharif, E. Pelinovsky, and A. Slunyaev, *Rogue waves in the ocean, observation, theories and modeling* (Advances in Geophysical and Environmental Mechanics and Mathematics Series, Springer, Heidelberg, 2009).
- [11] A. Osborne, *Nonlinear ocean waves* (Academic Press, 2010).
- [12] D. H. Peregrine, Water waves, nonlinear Schrödinger equations and their solutions, *J. Aust. Math. Soc. Series B, Appl. Math.* **25**, 16 (1983).
- [13] N. N. Akhmediev and V. I. Korneev, Modulation instability and periodic solutions of the nonlinear Schrödinger equation, *Teoret. Mat. Fiz.* **69**, 1089 (1986).
- [14] E. A. Kuznetsov, Solitons in a parametrically unstable plasma, *DoSSR* **236**, 575 (1977).
- [15] Y.-C. Ma, The perturbed plane-wave solutions of the cubic Schrödinger equation, *Stud. Appl. Math.* **60**, 43 (1979).
- [16] M. Tajiri and Y. Watanabe, Breather solutions to the focusing nonlinear Schrödinger equation, *Phys. Rev. E* **57**, 3510 (1998).
- [17] B. Kibler, J. Fatome, C. Finot, G. Millot, F. Dias, G. Genty, N. Akhmediev, and J. M. Dudley, The Peregrine soliton in nonlinear fibre optics, *Nat. Phys.* **6**, 790 (2010).
- [18] A. Chabchoub, N. P. Hoffmann, and N. Akhmediev, Rogue wave observation in a water wave tank, *Phys. Rev. Lett.* **106**, 204502 (2011).
- [19] G. F. Clauss, M. Klein, and M. Onorato, Formation of extraordinarily high waves in space and time, in *International Conference on Offshore Mechanics and Arctic Engineering*, Vol. 44342 (2011) pp. 417–429.
- [20] H. Bailung, S. S. K., and N. Y., Observation of Peregrine solitons in a multicomponent plasma with negative ions, *Phys. Rev. Lett.* **107**, 255005 (2011).
- [21] B. Kibler, J. Fatome, C. Finot, G. Millot, G. Genty, B. Wetzl, N. Akhmediev, F. Dias, and J. M. Dudley, Observation of Kuznetsov-Ma soliton dynamics in optical fibre, *Sci. Rep.* **2**, 463 (2012).
- [22] B. Frisquet, B. Kibler, and G. Millot, Collision of Akhmediev breathers in nonlinear fiber optics, *Phys. Rev. X* **3**, 041032 (2013).
- [23] A. Chabchoub, N. Hoffmann, E. Tobisch, T. Waseda, and N. Akhmediev, Drifting breathers and Fermi–Pasta–Ulam paradox for water waves, *Wave Motion* **90**, 168 (2019).
- [24] D. S. Agafontsev and A. A. Gelash, Rogue waves with rational profiles in unstable condensate and its solitonic model, *Front. Phys.* **9**, 610896 (2021).
- [25] D. S. Agafontsev, S. Randoux, and P. Suret, Extreme rogue wave generation from narrowband partially coherent waves, *Phys. Rev. E* **103**, 032209 (2021).
- [26] A. A. Gelash and D. S. Agafontsev, Strongly interacting soliton gas and formation of rogue waves, *Phys. Rev. E* **98**, 042210 (2018).
- [27] A. Chabchoub, A. Slunyaev, N. Hoffmann, F. Dias, B. Kibler, G. Genty, J. M. Dudley, and N. Akhmediev, The Peregrine breather on the zero-background limit as the two-soliton degenerate solution: An experimental study, *Front. Phys.* **9**, 633549 (2021).
- [28] A. Chowdury, W. Chang, and M. Battiato, From rogue wave solution to solitons, *Phys. Rev. E* **107**, 014212 (2023).
- [29] A. Chowdury, W. Chang, and M. Battiato, Higher-order rogue wave fission under the effects of third-order dispersion, self-steepening and self-frequency shift, *arXiv preprint arXiv:2210.00426* (2022).
- [30] A. Gelash, D. Agafontsev, P. Suret, and S. Randoux, Solitonic model of the condensate, *Phys. Rev. E* **104**, 044213 (2021).
- [31] D. J. Kedziora, A. Ankiewicz, and N. Akhmediev, Rogue waves and solitons on a cnoidal background, *Eur. Phys. J.: Spec. Top.* **223**, 43 (2014).
- [32] F. Baronio, M. Conforti, A. Degasperis, S. Lombardo, M. Onorato, and S. Wabnitz, Vector rogue waves and baseband modulation instability in the defocusing regime, *Phys. Rev. Lett.* **113**, 034101 (2014).
- [33] J. Chen, D. E. Pelinovsky, and R. E. White, Rogue waves on the double-periodic background in the focusing nonlinear Schrödinger equation, *Phys. Rev. E* **100**, 052219 (2019).
- [34] W.-J. Che, S.-C. Chen, C. Liu, L.-C. Zhao, and N. Akhmediev, Nondegenerate Kuznetsov-Ma solitons of Manakov equations and their physical spectra, *Phys. Rev. A* **105**, 043526 (2022).
- [35] A. Gelash and A. Raskovalov, Vector breathers in the Manakov system, *Stud. Appl. Math.* **150**, 841 (2023).
- [36] M. A. Hofer, A. Mucalica, and D. E. Pelinovsky, KdV breathers on a cnoidal wave background, *J. Phys. A Math. Theor.* **56**, 185701 (2023).
- [37] N. Akhmediev, A. Ankiewicz, and J. M. Soto-Crespo, Rogue waves and rational solutions of the nonlinear Schrödinger equation, *Phys. Rev. E* **80**, 026601 (2009).
- [38] V. E. Zakharov and A. A. Gelash, Nonlinear stage of modulation instability, *Phys. Rev. Lett.* **111**, 054101 (2013).
- [39] A. A. Gelash and V. E. Zakharov, Superregular solitonic solutions: a novel scenario for the nonlinear stage of modulation instability, *Nonlinearity* **27**, R1 (2014).
- [40] B. Kibler, A. Chabchoub, A. Gelash, N. Akhmediev, and V. E. Zakharov, Superregular breathers in optics and hydrodynamics: omnipresent modulation instability beyond simple periodicity, *Phys. Rev. X* **5**, 041026 (2015).
- [41] M. J. Ablowitz and H. Segur, *Solitons and the inverse scattering transform*, Vol. 4 (SIAM, Philadelphia, 1981).
- [42] S. Novikov, S. V. Manakov, L. P. Pitaevskii, and V. E. Zakharov, *Theory of solitons: the inverse scattering method* (Springer Science & Business Media, New York, 1984).
- [43] V. E. Zakharov and A. B. Shabat, Exact theory of two-dimensional self-focusing and one-dimensional self-modulation of waves in nonlinear media, *Sov. Phys. JETP* **34**, 62 (1972).
- [44] L. D. Landau and E. M. Lifshitz, *Quantum Mechanics: Non-relativistic Theory. V. 3 of Course of Theoretical Physics* (Pergamon Press, 1958).
- [45] Z. Lewis, Semiclassical solutions of the Zaharov-Shabat scattering problem for phase modulated potentials, *Phys. Lett. A* **112**, 99 (1985).

- [46] R. Jenkins and K. D. T.-R. McLaughlin, Semiclassical limit of focusing NLS for a family of square barrier initial data, *Commun. Pure Appl. Math.* **67**, 246 (2014).
- [47] V. B. Matveev and M. A. Salle, *Darboux transformations and solitons* (Springer-Verlag, Berlin, 1991).
- [48] N. N. Akhmediev and N. V. Mitzkevich, Extremely high degree of N-soliton pulse compression in an optical fiber, *IEEE J. Quantum Electron.* **27**, 849 (1991).
- [49] V. E. Zakharov and A. V. Mikhailov, Relativistically invariant two-dimensional models of field theory which are integrable by means of the inverse scattering problem method, *Sov. Phys. JETP* **47**, 1017 (1978).
- [50] N. Akhmediev, J. M. Soto-Crespo, and A. Ankiewicz, Extreme waves that appear from nowhere: on the nature of rogue waves, *Phys. Lett. A* **373**, 2137 (2009).
- [51] A. Gelash, D. Agafontsev, V. Zakharov, G. El, S. Randoux, and P. Suret, Bound state soliton gas dynamics underlying the noise-induced modulational instability, *Phys. Rev. Lett.* **123**, 234102 (2019).
- [52] T. V. Tarasova and A. V. Shunyaev, Properties of synchronous collisions of solitons in the Korteweg–de Vries equation, *Commun. Nonlinear Sci. Numer. Simul.* **118**, 107048 (2023).
- [53] G. Xu, A. Gelash, A. Chabchoub, V. Zakharov, and B. Kibler, Breather wave molecules, *Phys. Rev. Lett.* **122**, 084101 (2019).
- [54] S. V. Manakov, Nonlinear Fraunhofer diffraction, *Zh. Eksp. Teor. Fiz* **65**, 10 (1973).
- [55] M. Klaus and J. K. Shaw, Purely imaginary eigenvalues of Zakharov-Shabat systems, *Phys. Rev. E* **65**, 036607 (2002).
- [56] E. N. Tsoy and F. K. Abdullaev, Interaction of pulses in the nonlinear Schrödinger model, *Phys. Rev. E* **67**, 056610 (2003).
- [57] M. Desaix, D. Anderson, L. Helczynski, and M. Lisak, Eigenvalues of the Zakharov-Shabat scattering problem for real symmetric pulses, *Phys. Rev. Lett.* **90**, 013901 (2003).
- [58] D. S. Agafontsev and V. E. Zakharov, Integrable turbulence and formation of rogue waves, *Nonlinearity* **28**, 2791 (2015).
- [59] G. Xu, A. Chabchoub, D. E. Pelinovsky, and B. Kibler, Observation of modulation instability and rogue breathers on stationary periodic waves, *Phys. Rev. Res.* **2**, 033528 (2020).
- [60] P. Dubard and V. B. Matveev, Multi-rogue waves solutions: from the NLS to the KP-I equation, *Nonlinearity* **26**, R93 (2013).
- [61] D. J. Kedziora, A. Ankiewicz, and N. Akhmediev, Classifying the hierarchy of nonlinear-Schrödinger-equation rogue-wave solutions, *Phys. Rev. E* **88**, 013207 (2013).
- [62] A. A. Gelash, Formation of rogue waves from a locally perturbed condensate, *Phys. Rev. E* **97**, 022208 (2018).
- [63] A. Gelash, G. Xu, and B. Kibler, Management of breather interactions, *Phys. Rev. Res.* **4**, 033197 (2022).
- [64] J. M. Dudley, G. Genty, and S. Coen, Supercontinuum generation in photonic crystal fiber, *Rev. Modern Phys.* **78**, 1135 (2006).
- [65] D. R. Solli, C. Ropers, P. Koonath, and B. Jalali, Optical rogue waves, *Nature* **450**, 1054 (2007).